FULL PAPER

Thermodynamics of Cr(VI) Adsorption on Magnetic Core-Shell Nanoparticles

Alex Fabiano Cortez Campos*, Fabiana Narciso da Silva, Marcelo Rubens Braga de Almeida, Luana Cristina Alves Sales, Paulo Henrique Michels-Brito, and Helena Augusta Lisboa de Oliveira

Laboratório de Nanociência Ambiental e Aplicada, Faculdade UnB – Planaltina, Universidade de Brasília, Planaltina, 73345-010, Brazil.

Abstract:

This work focuses on the influence of temperature on Cr(VI) adsorption by nanoadsorbents based on core-shell bimagnetic $CoFe_2O_4@\gamma\text{-}Fe_2O_3$ nanoparticles. The nanoadsorbents were synthesized using the hydrothermal coprecipitation method in alkaline medium followed by a surface treatment with $Fe(NO_3)_3$. The effect of initial chromium concentration and temperature of adsorption were evaluated from batch studies using 0.7 g/L of the nanoadsorbents. The results were analyzed in the framework of the Langmuir and Freundlich models and showed that the nanoadsorbents removed more than 95% of Cr(VI) in pH = 2.5 for a contact time of 30 min. The thermodynamics of the adsorption process was investigated by means of calculation of the Gibbs free energy, enthalpy and entropy changes. The results revealed that the Cr(VI) adsorption process is spontaneous, endothermic and presents an increase in randomness at the solid-solution interface.

Keywords: Cr(VI) adsorption; magnetic nanoadsorbents; thermodynamic parameters

1. Introduction

The intensive and inappropriate use of water resources related to the growing rate of industrialization has become an increasingly serious problem, mainly due to the release of polluted effluents in the environment [1]. In the case of electroplating and tannery industries, they generate liquid waste with a complex chemical composition largely containing heavy metals [2, 3]. Among these kinds of pollutants, hexavalent chromium (Cr(VI)) is considered highly toxic not only for the environment but also for humans. In fact, Cr(VI) acts as a carcinogen, mutagen, and teratogen agent in humans since it is able to permeate biological membranes causing damage to the DNA structure [4, 5]. In this context, Cr(VI) is one of the most investigated metals in the literature, and its removal of industrial wastewater has gained great attention in the area of environmental protection [6].

In recent years, several technologies have been developed to remove Cr(VI) from liquid effluents such as adsorption, chemical precipitation, electrochemical reduction, ion exchange, solvent extraction and reverse osmosis [7,8]. Adsorption methods present some important advantages when compared to other strategies in terms of low process cost, ease of operation, simplicity of design and high-energy efficiency [9,10]. Magnetic nanoadsorbents have demonstrated promising and effective results in Cr(VI) removal from water because they combine the spatial confinement of the adsorbent to the nanoscale with the possibility of magnetic manipulation [11]. Indeed, magnetically assisted chemical separation allows the treatment of a large mass of wastewater in a very short period and without generation of secondary waste. Moreover, the treatment can be conducted in either batch or continuous flow systems [12, 13].

The removal efficiency of the magnetic nanoadsorbents depends on several parameters including pH, contact time, shaking rate and

---

*Corresponding author. E-mail: relex@unb.br

particle mean size [14]. Temperature is also a key factor in the adsorption process, but it is rarely addressed in the literature with due depth, especially in adsorption processes using low-cost adsorbents [15]. As most of the polluted effluents are not found under ordinary temperature, the influence of the thermal variations on the adsorption process must be considered to better understand its mechanism and to design a sustainable adsorption system [16].

In this context, the main goal of the present paper is to investigate the influence of the temperature on Cr(VI) adsorption from aqueous solutions using nanoadsorbents based on core-shell bimagnetic ferrite nanoparticles ($CoFe_2O_4@\gamma-Fe_2O_3$). These novel nanoadsorbents are composed of a strongly responsive magnetic core surrounded by a highly sorptive surface layer of maghemite. The thermodynamics of the adsorption process is explored by means of calculation of the Gibbs free energy, enthalpy and entropy changes, which provide important insights into the overall mechanism of Cr(VI) adsorption.

2. Results and Discussion

Figure 1(a) shows the obtained diffraction pattern of the nanoadsorbent, which exhibits several lines corresponding to the characteristic interplanar spacings [220], [311], [400], [422], [511] and [440] of the spinel structure. The mean size of the nanoadsorbent was determined by using the Scherrer's formula applied to the most intense [311] line [17]. Figure 1(b) and 1(c) respectively exhibit a typical TEM image of the nanoadsorbent, and the corresponding size distribution, which was evaluated considering approximately 500 nanoparticles and fitted by a log-normal law. As it can be seen, the nanoadsorbents appear roughly spherical and presenting a usual intrinsic polydispersity. The results of the structural and physicochemical characteristics of the nanoadsorbent are collected in Table 1. The size of the cubic cell was found equal to *a* = 0.832 nm which well agrees with the value of International Centre for Diffraction Data (ICDD) *a* = 0.839 nm for cobalt bulk material (ICDD 00-022-1086).

The amphoteric behavior of the nanoadsorbent surface sites leads to positive,

neutral or negative charge depending on the pH of the medium [18, 19]. In acidic medium, the nanoadsorbent surface mostly presents $\equiv FeOH_2^+$ sites, which is consistent with the zeta potential result [20, 21]. As a consequence, the process of Cr(VI) adsorption onto the magnetic nanoadsorbent mainly involves strong electrostatic interactions between $\equiv FeOH_2^+$ sites and $HCrO_4^-/Cr_2O_7^{2-}$, which are the predominant Cr(VI) species at pH = 2.5 [22, 23].
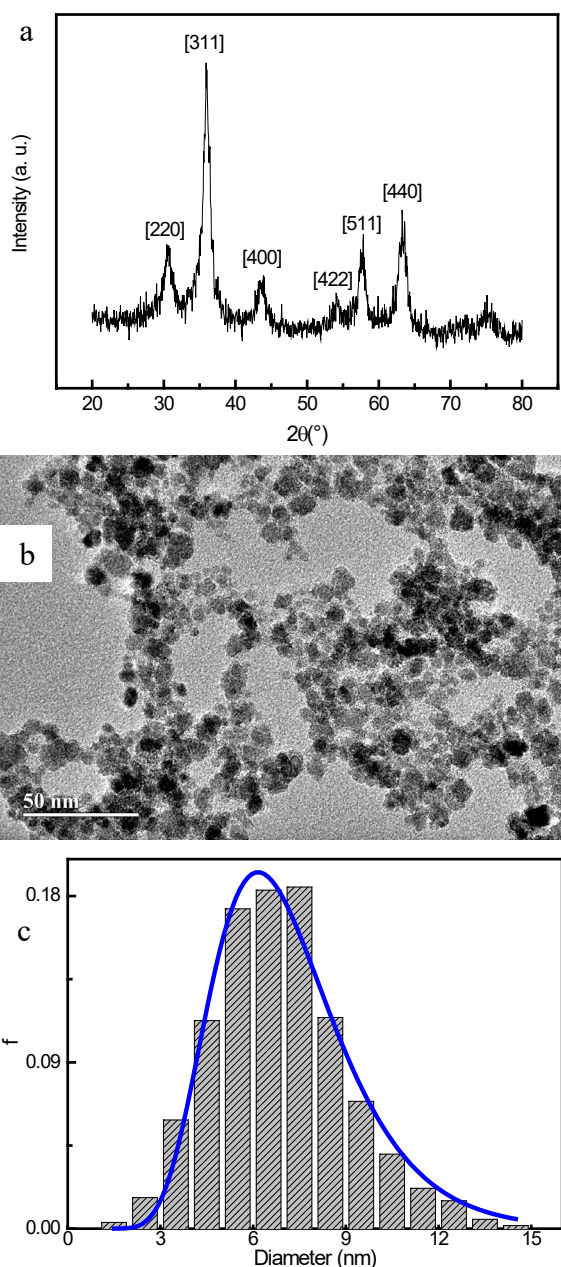
Figure 1. (a) X-ray powder diffraction pattern of the nanoadsorbent. (b) TEM image with the (c) corresponding normalized histogram of the nanoparticles size distribution.

65

Orbital: Electron. J. Chem. 11 (2): 64-70, 2019

Table 1. Structural and physicochemical characteristics of the nanoadsorbent: mean size obtained from XRD (d_{XR}), lattice parameter (a), characteristic diameter obtained from TEM (d_0), polydispersity (s), maghemite shell fraction (ϕ_s/ϕ_p) and zeta potential (ζ).

d_{XR} (nm)	a (nm)	d_0 (nm)	s	ϕ_s/ϕ_p	ζ (mV)
7.5	0.832	7.1	0.3	0.41	+77.1

Figure 2 exhibits the fitting of the equilibrium data for Cr(VI) adsorption using the linearized forms of Langmuir and Freundlich models [24], which can be respectively expressed as

$$\frac{C_e}{q_e} = \frac{C_e}{q_{max}} + \frac{1}{K_L q_{max}} , \qquad (1)$$

$$\ln q_e = \ln K_F + \frac{1}{n} \ln C_e , \qquad (2)$$

where q_{max} corresponds to the maximum adsorption capacity, K_L is the Langmuir constant (related to the adsorption energy), K_F is the Freundlich constant (related to the adsorption capacity) and $1/n$ is a heterogeneity factor which accounts for adsorption intensity. The obtained fitted parameters are listed in Table 2. The percentage of Cr(VI) removal was higher than 95% in the experimental conditions, confirming the efficiency of the nanoadsorbent.

According to the correlation coefficients, the adsorption data showed a better compliance with the Freundlich model, indicating that the Cr(VI) adsorption occurs in multilayers and that the nanoadsorbents surface presents a heterogeneous energy distribution. The parameter n lied in the range of 1-10 confirming a favorable adsorption process [25–27]. The

formation of the multilayers can be explained as a result of the strong local electrostatic field existing around the nanoadsorbent surface, which induces a strong accumulation of anionic Cr(VI) species [28].
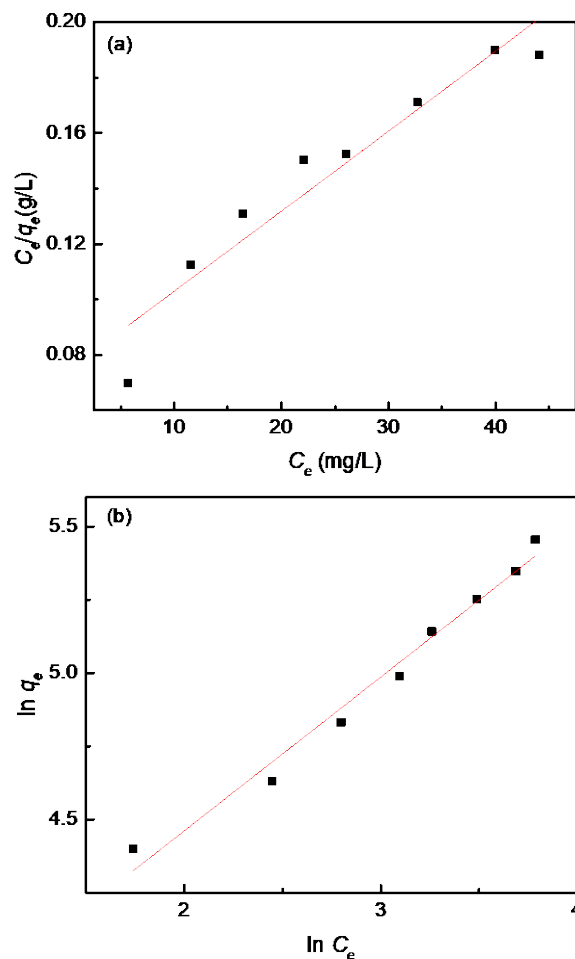
Figure 2. Fitting of equilibrium adsorption data using linearized Langmuir (a) and Freundlich (b) models.

Table 2. Parameters for Cr(VI) adsorption obtained from linearized Langmuir and Freundlich models.

Langmuir Model		Freundlich Model	
K_L (L mg^{-1})	0.039	K_F (mg$^{1-1/n}$ g^{-1} L$^{1/n}$)	30.3
q_{max} (mg g^{-1})	346.4	n	1.9
R^2	0.9236	R^2	0.9806

The spontaneity of the Cr(VI) adsorption was evaluated from the Gibbs free energy change (ΔG^0), calculated at equilibrium conditions as

$$\Delta G^0 = -RT \ln K , \qquad (3)$$

where R is the universal gas constant (8.314 J K^{-1} mol^{-1}), T is the absolute temperature and K

corresponds to the thermodynamic equilibrium constant, which can be related to the Freundlich constant through the equation [29, 30].

$$K = K_F \rho \left(\frac{10^6}{\rho} \right)^{(1-1/n)} , \qquad (4)$$

66

Orbital: Electron. J. Chem. 11 (2): 64-70, 2019

where ρ is the density of distilled water (in units of g mL^{-1}). Thus, the change in standard enthalpy (ΔH^0) and entropy (ΔS^0) of the adsorption process were calculated using the van't Hoff equation:

$$\ln K = -\frac{\Delta H^0}{RT} + \frac{\Delta S^0}{R}, \qquad (5)$$

from the slope and the intercept of plots of ln K versus $1/T$, respectively (Figure 3). The results are listed in table 3.
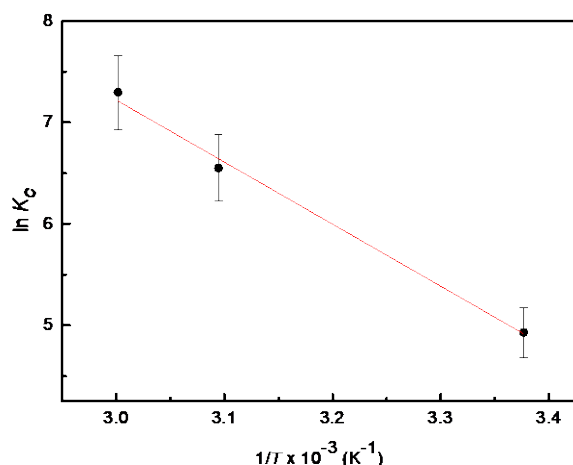
Figure 3. van't Hoff plots of Cr(VI) adsorption onto magnetic nanoadsorbents (R^2 = 0.9918)

Table 3. Thermodynamic parameters of Cr(VI) adsorption.

T (K)	$\Delta G°$ (kJ mol^{-1})	$\Delta H°$ (kJ mol^{-1})	$\Delta S°$ (J mol^{-1} K^{-1})
296.15	-12.1		
323.15	-17.6	50.8	212.5
333.15	-20.2		

The negative values of the Gibbs free energy change confirm the feasibility and the spontaneity of the Cr(VI) adsorption. Also, since ΔG^0 becomes more negative with the temperature increase, the adsorption process is enhanced at higher temperatures. The enthalpy change was positive revealing that the interaction of Cr(VI) species with the nanoadsorbent is endothermic in nature. It can be enlightened considering that the adsorbing Cr(VI) species (HCrO$_4^-$ and Cr$_2$O$_7^{2-}$) must lose part of their hydration shell to attach onto nanoadsorbent surface. The energy consumed in this process exceeds the energy released when the Cr(VI) species are effectively adsorbed [28,31,32]. Regarding the entropy

change, its positive value indicates an increase of disorder in the solid/solution interface related to the Cr(VI) adsorption. This randomness increase can be ascribed as an extra translational entropy gained by the released solvent molecules which were previously adsorbed onto nanoadsorbent [33]. The spontaneity, endothermicity and increased entropy observed in our adsorption experiments agree with previous works of Cr(VI) adsorption with other magnetic materials [34–36].

The heat evolved in the Cr(VI) adsorption can provide some important information related to the type of sorption involved in the process. The magnitude of ΔH^0 in physisorption is generally lower than 20 kJ/mol while in chemisorption it falls in a range of 80 to 200 kJ/mol [32]. In this context, our thermodynamic results suggest that the Cr(VI) removal at pH = 2.5 involves physical and chemical adsorption at the same time, as already observed in the case of other adsorbents for chromium [37–39]. It is consistent with the formation of the multilayers, where an inner layer of weakly chemisorbed Cr(VI) ions would be surrounded by adjacent layers of physisorbed hydrated Cr(VI) ions.

Another important thermodynamic parameter that provides relevant information about the heat exchanges in the adsorption process is the isosteric adsorption heat (ΔH_x), defined as the standard adsorption enthalpy change for a constant amount of adsorbate [29]. This thermodynamic parameter is an indicator of the performance of the adsorption process and the surface heterogeneity and can be calculated using the Clausius-Clapeyron equation:

$$\frac{d\left(\ln C_e\right)}{dT} = -\frac{\Delta H_x}{RT^2}. \qquad (6)$$

For small temperature variations, ΔH_x can be considered as temperature independent and the integrated form of the above equation can be expressed as:

$$\ln C_e = \frac{\Delta H_x}{R}\cdot\left(\frac{1}{T}\right) + C, \qquad (7)$$

where C is the constant of integration. Thus, the isosteric heat of Cr(VI) adsorption was calculated from the slope of plots of ln C_e x $1/T$ for different values of adsorption capacities (Figure 4). The isosteric curves for different C_e values and fixed

67

Orbital: Electron. J. Chem. 11 (2): 64-70, 2019

amount of adsorbate were obtained from the results of adsorption isotherms at different temperatures.
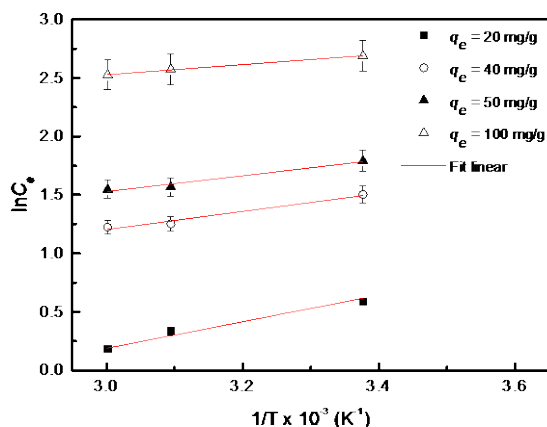
Figure 4. Isosteric plots for different surface coverages.

The positive values of ΔH_x reinforce the endothermic nature of the adsorption process. It is also important to comment that the isosteric adsorption heat values vary with the amount of Cr(VI) adsorbed, which corroborates the heterogeneity of the adsorption process [40,41]. According to the literature [42], the isosteric heat of adsorption is higher for low surface coverage and it steadily decreases with increasing q_e, as observed in our experiments.

Table 4. Results of isosteric heat of Cr(VI) adsorption.

q_e (mg/g)	ΔH_x (kJ/mol)
20	9.5
40	6.4
50	5.6
100	3.6

The qualitative results of our thermodynamic investigation are in good agreement with the literature for Cr(VI) removal using other adsorbents as activated carbon [43], graphene oxide [35] aluminum and magnesium hydroxides [34] and polymeric microbeads [44]. In all these surveys, the process of Cr(VI) adsorption was also spontaneous, endothermic and presented an increased randomness.

3. Material and Methods

3.1. Reagents and equipment

All reagents used in this survey were of analytical grade from Aldrich or Merck and therefore used without any further purification. Stock solutions of chromium (1000 mg/L) were prepared in deionized water Type I (Millipore Milli-Q Gradient quality). Solution pH were measured using a pH meter (model Q400AS, QUIMIS) with a pH glass double-junction electrode. The pH adjustments were carried out using solutions of HNO_3 (0.1 mol/L) and NaOH (0.1 mol/L). The adsorbent–adsorbate dispersions were agitated using an orbital shaker (Model DSR- 10B – Global Trade Technology) at constants speed and temperature. The experiments of adsorption capacity in function of temperature were performed in a temperature controlled shaker incubator (model Q226M, QUIMIS). The equilibrium concentrations of chromium were determined by flame atomic absorption spectroscopy (FAAS) at 357.9 nm wavelength (model S Series Thermo Scientific spectrometer) as well as the iron (372 nm) and cobalt (240.7 nm) concentrations to check the chemical composition of the elaborated nanomaterial. All the measurements were carried out in triplicate.

3.2. Nanoadsorbent elaboration

Cobalt ferrite nanoparticles ($CoFe_2O_4$) were synthesized by hydrothermal coprecipitation of aqueous solutions of cobalt (II) nitrate and iron (III) chloride in alkaline medium (methylamine), according to a well-known procedure [45,46]. Next, the precipitate was washed and hydrothermally treated with a solution of iron (III) nitrate to create a thin layer of maghemite (γ-Fe_2O_3) leading to the final nanoadsorbent ($CoFe_2O_4@\gamma$-Fe_2O_3). The maghemite shell protects the nanoparticle against particle dissolution in acid medium. The structure of this kind of core-shell nanoparticles has been extensively studied elsewhere [47–49].

3.3. Nanoadsorbent characterization

X-rays diffraction spectroscopy was employed to characterize the crystalline structure and the mean size of the nanoadsorbent. The measurements were performed using a diffractometer (model D8 Focus, Bruker) operated at 40 kV/30 mA with Cu Kα radiation (λ = 0.1541 nm) selected by a Ge(111) monochromator. The

68

Orbital: Electron. J. Chem. 11 (2): 64-70, 2019

spectra were recorded within a 20° ≤ 2θ ≤ 80° interval, with a 0.05° step and 0.1°/min scan rate. Transmission electron microscopy (TEM) were also performed to characterize the morphology and the size distribution of nanoadsorbents. The pictures were obtained with a JEOL JEM-2100 microscope under an accelerating voltage of 200 kV.

The chemical composition of the nanoadsorbents was checked using FAAS measurements. According to the core-shell model, it was possible to determine the maghemite shell fraction ϕ_s/ϕ_p, where ϕ_s and ϕ_p are the volume fractions of maghemite and nanoparticles, respectively [47].

The electrophoretic mobilities of the nanoadsorbents were determined at pH = 2.5 using a ZetaSizer (model NanoZS 90, Malvern) with a disposable cuvette (DTS 1070). The results were converted in zeta potential values (ζ) through the Henry equation [50].

3.4. Batch adsorption experiments

The adsorption experiments were carried out by following batch tests. A mass of 0.010 g of the nanoadsorbent was added to 15 mL of standard Cr(VI) solutions of varying concentrations (60-200 mg/L) under previously determined standard conditions (pH = 2.5, orbital shaking rate of 400 RPM, contact time of 30 minutes and at 25 °C) unless otherwise specified. After the equilibrium time, the nanoadsorbents loaded with Cr(VI) were separated from solution using a hand-held permanent magnet (Nd-Fe-B). The Cr(VI) concentration in the supernatant was determined by FAAS. Then, the amount of Cr(VI) adsorbed (mg/g) at equilibrium (q_e) was determined as:

$$q_e = \frac{(C_0 - C_e)}{m} V , \qquad (8)$$

and the percentage of removal was calculated by

$$\%\text{Removal} = \frac{(C_0 - C_e)}{C_0} \times 100\% , \quad (9)$$

where C_0 and C_e (mg/L) are the initial and equilibrium Cr(VI) concentration respectively, V (L) is the solution volume and m (g) is the nanoadsorbent mass.

The thermodynamic behavior of the adsorption process was investigated repeating the batch experiments for two other temperatures (50 and 60°C) in a temperature controlled shaker incubator.

4. Conclusions

Together with adsorption isotherm models, the investigated thermodynamic parameters offered relevant information about the mechanism of Cr(VI) removal by the core-shell bimagnetic nanoadsorbents. The batch adsorption experiments best followed the Freundlich model indicating that Cr(VI) species form multilayers around the surface of the elaborated magnetic nanoadsorbents. The obtained thermodynamic parameters revealed that the Cr(VI) adsorption is spontaneous and endothermic in nature. The adsorption was enhanced at higher temperatures and presented an increased entropy at the surface/solution interface. Finally, the prepared nanoadsorbents can be used as a powerful tool for Cr(VI) removal from contaminated water at high temperatures.

Acknowledgments

References and Notes

[1] Vasudevan, S.; Lakshmi, J.; Sozhan, G. *Desalination* **2011**, *275*, 260. [Crossref]

[2] Wang, P.; Lo, I. M. C. *Water Res.* **2009**, *43*, 3727. [Crossref]

[3] Thomas, O.; Decherf, H.; Touraud, E.; Baurès, E.; Pouet, M.-F. In *Techniques and Instrumentation in Analytical Chemistry*; Thomas, O., Burgess, C., Eds.; Amsterdam: Elsevier, 2007, chapter 9. [Crossref]

[4] Quievryn, G.; Messer, J.; Zhitkovich, A. *Biochemistry* **2002**, *41*, 3156. [Crossref]

[5] Lorena, D.; Ceballos, G.; Pinta-melo, J.; Hidalgo-bonilla, S. P.; Burbano-rosero, E. M. *Univ. y Salud* **2017**, *19*, 102. [Crossref]

[6] Yu, W.; Zhang, L.; Wang, H.; Chai, L. *J. Hazard. Mater.* **2013**, *260*, 789. [Crossref]

[7] Liu, Y.; Chen, M.; Yongmei, H. *Chem. Eng. J.* **2013**, *218*, 46. [Crossref]

69

Orbital: Electron. J. Chem. 11 (2): 64-70, 2019

[8] Lazaridis, N. K.; Bakoyannakis, D. N.; Deliyanni, E. A. *Chemosphere* **2005**, *58*, 65. [Crossref]

[9] Taghizadeh, M.; Hassanpour, S. *Polym.* **2017**, *132*, 1. [Crossref]

[10] Dawood, S.; Sen, T. K. *Water Res.* **2012**, *46*, 1933. [Crossref]

[11] Mehta, D.; Mazumdar, S.; Singh, S. K. *J. Water Process Eng.* **2015**, *7*, 244. [Crossref]

[12] Reddy, D. H. K.; Lee, S. M. *Adv. Colloid Interface Sci.* **2013**, *201–202*, 68. [Crossref]

[13] Hao, Y.-M.; Man, C.; Hu, Z.-B. *J. Hazard. Mater.* **2010**, *184*, 392. [Crossref]

[14] Aghaei, E.; Alorro, R.; Encila, A.; Yoo, K. *Metals* **2017**, *7*, 529. [Crossref]

[15] Ahsan, S.; Rahman, M. A.; Kaneco, S.; Katsumata, H.; Suzuki, T.; Ohta, K. *Clean Technol. Environ. Policy* **2005**, *7*, 198. [Crossref]

[16] Baig, S. A.; Sheng, T. T.; Sun, C.; Xue, X. Q.; Tan, L. S.; Xu, X. H. *PLoS One* **2014**, *9*, e100704. [Crossref]

[17] Hammond, C. *The Basics of Crystallography and Diffraction*, 3rd ed.; Oxford University Press: New York, 1997.

[18] Campos, A. F. C.; Medeiros, W. C. De; Aquino, R.; Depeyrot, J. *Mater. Res.* **2017**, *20*, 1729. [Crossref]

[19] Campos, A. F. C.; Tourinho, F. A.; Da Silva, G. J.; Lara, M. C. F. L.; Depeyrot, J. *Eur. Phys. J. E* **2001**, *6*, 29. [Crossref]

[20] Rajput, S.; Pittman, C. U.; Mohan, D. *J. Colloid Interface Sci.* **2016**, *468*, 334. [Crossref]

[21] Banerjee, S. S.; Chen, D. H. *J. Hazard. Mater.* **2007**, *147*, 792. [Crossref]

22] Pang, Y.; Zeng, G.; Tang, L.; Zhang, Y.; Liu, Y.; Lei, X.; Li, Z.; Zhang, J.; Liu, Z.; Xiong, Y. P. *Chem. Eng. J.* **2011**, *175*, 222. [Crossref]

[23] Hu, J.; Chen, G.; Lo, I. M. C. *Water Res.* **2005**, *39*, 4528. [Crossref]

[24] Foo, K. Y. F.; Hameed, B. H. *Chem. Eng. J.* **2010**, *156*, 2. [Crossref]

[25] Kahu, S. S.; Shekhawat, A.; Saravanan, D.; Jugade, R. M. *Carbohydr. Polym.* **2016**, *146*, 264. [Crossref]

[26] Brdar, M.; Šćiban, M.; Takači, A.; Došenović, T. *Chem. Eng. J.* **2012**, *183*, 108. [Crossref]

[27] Chowdhury, S. R.; Yanful, E. K. *J. Environ. Manage.* **2010**, *91*, 2238. [Crossref]

[28] Campos, A. F. C.; Oliveira, H. A. L. de; Silva, F. N. da; Silva, F. G. da; Coppola, P.; Aquino, R.; Mezzi, A.; Depeyrot, J. *J. Hazard. Mater.* **2019**, *362*, 82. [Crossref]

[29] Ghosal, P. S.; Gupta, A. K. *RSC Adv.* **2015**, *5*, 105889. [Crossref]

[30] Tran, H. N.; You, S. J.; Chao, H. P. *J. Environ. Chem. Eng.* **2016**, *4*, 2671. [Crossref]

[31] Yang, S.; Zhao, D.; Zhang, H.; Lu, S.; Chen, L.; Yu, X. *J. Hazard. Mater.* **2010**, *183*, 632. [Crossref]

[32] Anastopoulos, I.; Kyzas, G. Z. *J. Mol. Liq.* **2016**, *218*, 174. [Crossref]

[33] Nassar, N. N. *J. Hazard. Mater.* **2010**, *184*, 538. [Crossref]

[34] Li, Y.; Gao, B.; Wu, T.; Sun, D.; Li, X.; Wang, B.; Lu, F. *Water Res.* **2009**, *43*, 3067. [Crossref]

[35] Wang, H.; Yuan, X.; Wu, Y.; Chen, X.; Leng, L.; Wang, H.; Li, H.; Zeng, G. *Chem. Eng. J.* **2015**, *262*, 597. [Crossref]

[36] Sharma, Y. C.; Srivastava, V. *J. Chem. Eng. Data* **2011**, *56*, 819. [Crossref]

[37] Lee, M. G.; Cheon, J. K.; Kam, S. K. *J. Ind. Eng. Chem* **2003**, *9*, 174.

[38] Al-Anber, M.; Al-Anber, Z. A. *Desalination* **2008**, *225*, 70–81. [Crossref]

[39] Al-Anber, M. *Asian J. Chem.* **2007**, *19*, 3493.

[40] Anirudhan, T. S.; Radhakrishnan, P. G. *J. Chem. Thermodyn.* **2008**, *40*, 702. [Crossref]

[41] Heidari, A.; Younesi, H.; Rashidi, A.; Ghoreyshi, A. A. *Chem. Eng. J.* **2014**, *254*, 503. [Crossref]

[42] Dąbrowski, A. *Adv. Colloid Interface Sci.* **2001**, *93*, 135. [Crossref]

[43] Arivoli, S.; Hema, M.; Karuppaiah, M.; Saravanan, S. *E-Journal Chem.* **2008**, *5*, 820. [Crossref]

[44] Kara, A.; Demirbel, E. *Water. Air. Soil Pollut.* **2012**, *223*, 2387. [Crossref]

[45] Tourinho, F. A.; Franck, R.; Massart, R. *J. Mater. Sci.* **1990**, *25*, 3249. [Crossref]

[46] Sousa, M. H.; Tourinho, F. A.; Depeyrot, J.; da Silva, G. J.; Lara, M. C. F. L. *J. Phys. Chem. B* **2001**, *105*, 1168. [Crossref]

[47] Gomes, J. A.; Sousa, M. H.; Tourinho, F. A.; Aquino, R.; Depeyrot, J.; Dubois, E.; Perzynski, R. *J. Phys. Chem. C* **2008**, *112*, 6220. [Crossref]

[48] Aquino, R.; Tourinho, F. A.; Itri, R.; E Lara, M. C. F. L.; Depeyrot, J. *J. Magn. Magn. Mater.* **2002**, *252*, 23. [Crossref]

[49] Pilati, V.; Cabreira Gomes, R.; Gomide, G.; Coppola, P.; Silva, F. G.; Paula, F. L. O.; Perzynski, R.; Goya, G. F.; Aquino, R.; Depeyrot, J. *J. Phys. Chem. C* **2018**, *122*, 3028. [Crossref]

[50] Bhattacharjee, S. *J. Control. Release* **2016**, *235*, 337. [Crossref]

70

Orbital: Electron. J. Chem. 11 (2): 64-70, 2019